Video SAR Moving Target Detection Using Dual Faster R-CNN

Liwu Wen [ID], Jinshan Ding [ID], *Member, IEEE*, and Otmar Loffeld [ID], *Senior Member, IEEE*

Abstract—Video synthetic aperture radar (SAR) has shown great potentials in detection and tracking of slow ground moving targets. The classical shadow-aided detection was applied in video SAR, and most recently, the deep learning approach has been developed for shadow-aided moving target detection. This article presents a joint moving target detection approach for video SAR using a dual faster region-based convolutional neural network (Faster R-CNN), which algorithmically combines the shadow detection in the SAR image and the Doppler energy detection in the range-Doppler (RD) spectrum domain, and this new approach can suppress false alarm sufficiently. Video SAR image and its corresponding low resolution RD spectrum are fed into the developed dual Faster R-CNN. A correct detection can be achieved if the shadow of a moving target and its Doppler energy are simultaneously detected by paired region proposals, which are obtained by sharing the region proposals of two independent region proposal networks (RPNs). Therefore, the performance of moving target detection can be significantly improved by using diverse features in different domains. This proposed approach has been verified by both the simulated and real video SAR data. Compared to other classical methods, our approach exhibits a great detection performance in terms of fewer false alarms and acceptable missing alarms.

Index Terms—Deep learning, ground moving target indication (GMTI), radar imaging, shadow detection, video synthetic aperture radar (SAR).

I. INTRODUCTION

VIDEO synthetic aperture radar (SAR) is a high frame rate imaging system that usually works in spotlight mode. The resulted sequential SAR images can be used to dynamically observe the area of interest [1], which have been found useful in surveillance, forward and backward tracking for ground moving target indication (GMTI), coherent or noncoherent change detection and 3-D imaging [2]–[4]. An early technical validation of video SAR was conducted in *Ku*-band by Sandia National Laboratory. A video SAR system operated at 235 GHz was discussed in [5], which was later integrated into the multispectral aiming system. Some efforts on video SAR image formation have been released as well [6]–[8].

The shadow appears due to the obstruction of target on the incident radar radiation [9]. The subaperture processing strategy is extensively used in video SAR, which implies a short beam dwell time. On the other hand, higher operation frequency makes the Doppler modulation of moving target more sensitive to its motion, and thus, the Doppler energy of target usually deviates from its real position. As a result, shadows can be more easily observed compared to the traditional SAR system [10]. It is very difficult to directly detect the moving target in SAR images, especially when its Doppler energy is smeared and shifted, which may be outside the scene as an extreme case [11]. On the contrary, the moving target can leave an observable shadow on its trajectory under the appropriate speed [12], which enables an indirect detection by finding this shadow. The features of moving target shadow, such as size, shape, and intensity, are very useful for target detection, location, and tracking. The shadow is more reliable for locating target rather than using Doppler energy [9] since it can approximately represent the real position of moving target in the short beam dwell time, and thus, the shadow-based detection can directly locate the moving target in the high-resolution SAR images, which avoids the complex relocation operation in classical SAR-GMTI algorithms. In addition, the multiframe information in video SAR can be used to obtain a better performance.

The current shadow-based detection methods are mainly based on classical image processing, including single-frame [13] and multiframe processing [14]–[17]. Shadow detection based on classical image processing has received much attention because of its independency of the number of channels. Liu [13] presented a local feature analysis method for shadow detection in a single-frame video SAR image. On the other hand, video SAR can provide continuous moving target shadows. Zhang [14] discussed a classical shadow detection approach that includes adjacent image registration, speckle noise suppression, background extraction, differential processing, morphological processing, and connected component detection. Tian [16] used the track-before-detect (TBD) algorithm to deal with the moving target detection and tracking in the video SAR sequential images.

Moreover, the shadow detection combined with the SAR-GMTI technique has also been concerned. Xu [11] presented a framework based on enhanced shadow-aided decision for multichannel SAR-GMTI, which, however, relies on multichannel returns to estimate the cross-track velocity to correct the azimuth displacement and achieve the relocation of target.

The target detection based on the deep convolutional neural network (DCNN) has achieved a remarkable performance in optical images [18]–[20], and also in the field of video target detection [21], [22]. Recently, some target detection and tracking algorithms based on DCNN have been successfully applied to radar [23]–[26]. The traditional target detection algorithms usually suffer a lot from complicate clutter background and low signal-to-clutter ratio (SCR). Alternatively, DCNN can automatically extract features from data for the use of detection, recognition, and tracking, which removes some limitations of traditional methods.

In video SAR images, the moving target shadow is a typical dim target with low intensity and simple features, which has no obvious differences from other weak reflectivity areas. In most cases, the size and intensity of shadow are time-varying due to target motion and change of observing angle. As a result, false alarms are very common in the detection. On the other hand, the generation of shadow strongly depends on target motion, especially for fast maneuvering target whose shadow boundary is blurred and exhibits low contrast with the background. Additionally, the ambiguous or smeared Doppler energy of target may mask its shadow in some extreme cases. These issues give rise to the missing alarms in some frames. Furthermore, practical implementation of deep learning technology in radar is hampered in many cases by a severe shortage of appropriate training data, and therefore, the joint detection, which makes full use of different features becomes a concern in radar applications.

The main contributions of this article are threefold.

1) We propose a new joint detection approach based on the developed dual faster region-based convolutional neural network (Faster R-CNN), which benefits from combining the shadow detection in SAR image and Doppler energy detection in range-Doppler (RD) spectrum domain.

2) In the designed dual Faster R-CNN, a high resolution SAR image and its corresponding low resolution RD spectrum are simultaneously input, and two independent region proposal networks (RPNs) are used to generate proposals on SAR image and RD spectrum, respectively.

3) We propose a rule-based azimuth coordinate shift method to shift proposals from one domain to the other, and thus, the paired proposals can be obtained, which drive the network to detect moving targets around the same range of SAR image and RD spectrum. Hence, a correct detection can be declared if the shadow of a moving target and its Doppler energy are simultaneously detected.

This proposed approach has been verified by both the simulated and real video SAR data. Compared to the classical Faster R-CNN and conventional dynamic programming-based TBD (DP-TBD) algorithm, our approach exhibits a great detection performance of moving target with few false alarms and acceptable missing alarms.

The rest of this article is organized as follows. Section II briefly discusses the classical Faster R-CNN for detection in the SAR image and its limitations. The proposed joint detection approach using dual Faster R-CNN are detailed in Section III. Section IV presents the detection results of dual Faster R-CNN. Section V concludes this article.
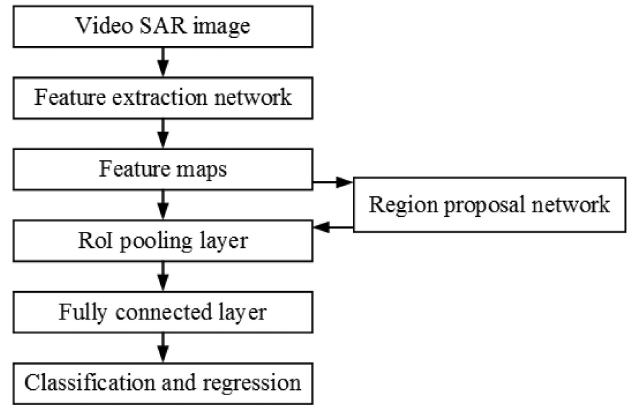

Fig. 1.   Flowchart of the classical Faster R-CNN for shadow detection.

II. Shadow Detection in SAR Image

A. Faster R-CNN for Detection

R-CNN has achieved a great success in the field of target detection in optical images [18]. However, it is not an end-to-end detection network. In order to solve the problems of slow training speed and inaccurate detection, fast R-CNN uses CNN to extract features from the whole image and maps region proposals to the feature maps [19]. However, both R-CNN and fast R-CNN use selective search algorithm to generate region proposals, which have the disadvantages of slow generation speed and redundant features.

Therefore, the RPN is proposed in Faster R-CNN. It uses the fully convolutional network to provide region proposals and shares feature maps with the detection network, which greatly improves the speed and accuracy of the generations of region proposals [20]. The flowchart of the classical Faster R-CNN for shadow detection in video SAR is shown in Fig. 1.

B. Limitations of Image Detection

Both the false alarms and missing alarms are important concerns in shadow detection. Moving target shadows are mostly dim targets in video SAR images, which challenge the Faster R-CNN. The low resolution makes the features of shadow simple, and the shadow often appears as dark area with blurred boundary. Therefore, other weak reflectivity areas, such as the shadows of fixed targets, add to false alarms.

On the other hand, the size, shape, and intensity of a shadow are greatly affected by the motion of target. When the target stops, its shadow becomes difficult to observe. For a fast maneuvering target, the occlusion time of target to the background becomes shorter in the subaperture integration time, and thus, the shadow sometimes cannot be observed. In addition, it is possible for the ambiguous or smeared Doppler energy to mask its or other shadows in some frames. All these factors may result in missing alarms.

It has been found that the classical Faster R-CNN has an acceptable false alarm rate in moving target shadow detection, provided that large training data are used, particularly when the testing data have the same distribution as the training data, such
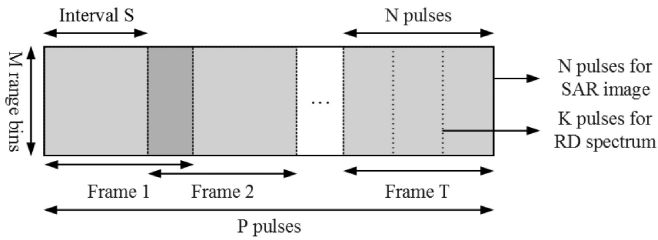
Fig. 2.   Acquisition of sequential video SAR images and RD spectra.

(a)   (b)

Fig. 3.   Schematic diagram of moving target detection combined shadow and Doppler energy. (a) Slow moving target. (b) Fast moving target.

as using the same or similar scenes. However, the missing alarms are still inevitable. In addition, the generalization ability of the classical Faster R-CNN is quite poor. For an unknown scene that is not used in the training dataset, the detection performance deteriorates seriously, resulting in a large number of false alarms.

III. JOINT DETECTION USING DUAL FASTER R-CNN

We propose an image-based end-to-end dual Faster R-CNN to improve the shadow-based moving target detection in video SAR, which jointly utilizes the features of a moving target in SAR image and RD spectrum for robust detection.

A. Signal Model

Video SAR usually has a long observation time for continuous surveillance of the scene. As shown in Fig. 2, the complex returns are arranged as a matrix with M range bins and P pulses. Assume that there are N ($N \ll P$) pulses in each frame, the whole complex returns can be divided into T frames by using a sliding window (SW) whose interval equals to S ($S \leq N$).

The SAR image is obtained from N pulses using the polar format algorithm (PFA), which is a common image formation algorithm for spotlight SAR. The PFA reformats the measured SAR data to Cartesian data location array by interpolation and uses the 2-D fast Fourier transform to realize image formation [27]. K continuous pulses are extracted around the subaperture center, and the corresponding RD spectrum can be obtained after range compression and azimuth Fourier transform. Note that the classical clutter suppression methods are not used in our simulation, and therefore, the stationary clutter spectrum is retained. With the sliding of the window, sequential high resolution video SAR images and corresponding low resolution RD spectra are obtained.

B. Target Detection Combined Shadow and Doppler Energy

A shadow-aided multichannel SAR-GMTI method has been proposed [11], which relies on multichannel returns to relocate the detected targets and then combines with the detected shadows for joint decision. Instead, we propose a DCNN-based joint detection approach for the video SAR system, and the principle of this approach is illustrated in Fig. 3.

The video released by Sandia National Laboratories [28] demonstrates the idea of moving target detection combined shadow and Doppler energy. For a real moving target, its Doppler energy can be observed in the RD spectrum. Meanwhile, the
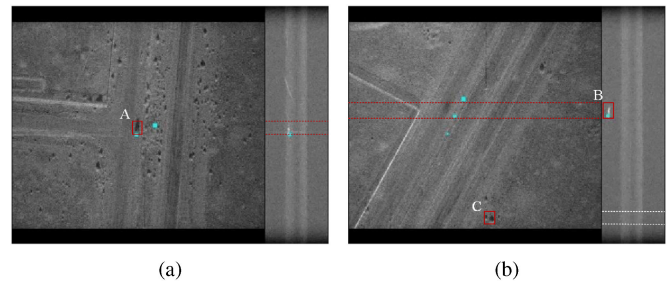
shadow appears in the SAR image due to obstruction of the target on the incident radar radiation and Doppler shift, which makes the defocused moving target image deviates from its real position. Therefore, a real moving target owns both the shadow and Doppler energy, which are located around the same range. Based on this property, a moving target can be jointly detected in the SAR image and RD spectrum.

In the real SAR video, there is only one moving target in the scene, therefore, we use two video SAR images corresponding to the initial and acceleration stages of this moving target to illustrate the detection principle of slow and fast moving targets, respectively. For a slow moving target shown in Fig. 3(a), the occlusion time to the background is longer in the subaperture integration time. Therefore, the contrast between its shadow and background is strong and the boundary is clear. In this case, the region proposal A provided by RPN will have high confidence to detect this shadow in SAR image. Assume that the position of its Doppler energy in the RD spectrum is limited by the red dotted line, we can shift the proposal A into the limited area in the RD spectrum to search the Doppler energy of moving target. Once it is detected, a reliable detection is declared. On the other hand, for the fast moving target shown in Fig. 3(b), the Doppler energy in the RD spectrum is reliable for target detection, while its shadow is hard to be detected due to the blurred boundary. The region proposal B correctly covers the Doppler energy, and the position of moving target shadow in the SAR image is also limited by the red dotted line. The joint detection is helpful for detecting the blurred shadow in this case by driving the neural network to search moving target shadow in the limited area, which has some improvements in missing alarm compared to SAR image-based detection. In addition, suppose that a region proposal C in the SAR image is a false alarm. Although it is very likely to be classified as a moving target shadow, the Doppler energy will not be detected in the RD spectrum, which is limited by the white dotted line. Therefore, this false alarm can be effectively suppressed.

C. Design of Dual Faster R-CNN

A dual Faster R-CNN is proposed to simultaneously detect the moving target in SAR image and RD spectrum, and the specific structure is given in Fig. 4.

In the preprocessing, all true targets are divided into the following three categories: shadow (visible moving target shadow
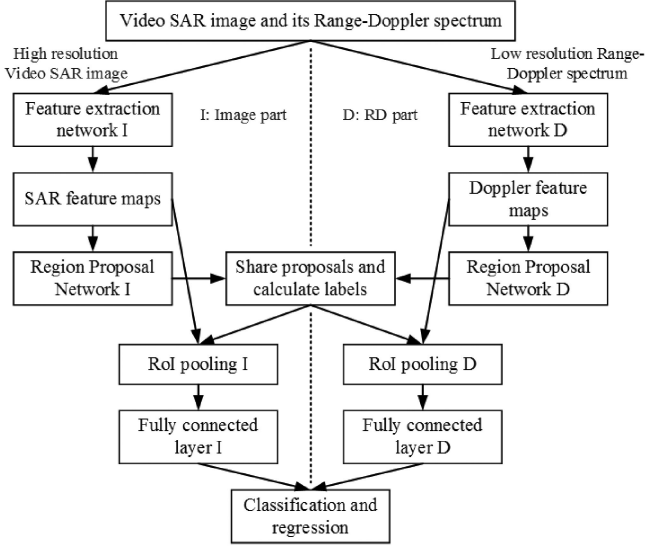
Fig. 4. Structure of the developed dual Faster R-CNN used for the robust detection of moving target in video SAR.

in image), masked shadow (invisible moving target shadow in image), and target Doppler (Doppler energy of moving target in RD spectrum). In the RD spectrum, although the changes in the velocity of moving target will lead to different broadening of its Doppler, the Doppler features will not change a lot due to low Doppler resolution. Therefore, the Doppler energy is both labeled as target Doppler whether it is inside or outside the stationary clutter spectrum. On the other hand, both the visible and invisible moving target shadows should be labeled in the SAR image. However, in some cases, the shadow will be masked by the Doppler energy of target in the image, resulting in changes of shadow features. Hence, the different shadows are labeled as shadow and masked shadow to distinguish this difference, respectively.

The high-resolution video SAR image and its related RD spectrum are fed into the developed dual Faster R-CNN simultaneously, and thus, the input is the concatenated image $\Omega = \{\alpha, \beta\}$ with the size of $H \times 2W$, where α and β are video SAR image and RD spectrum with the sizes of $H \times W$, respectively. Subsequently, the concatenated image Ω is divided into two parts after it is fed into the network. The video SAR image α and the ground-truth information of shadow and masked shadow are transmitted into the image part of the dual Faster R-CNN while the RD spectrum β and target Doppler are fed into the RD part.

The deep features of α and β are extracted by two independent feature extraction networks, and thus, SAR feature maps and Doppler feature maps are obtained, respectively. The popular VGG-16 network [29] is used as the feature extraction network in this article.

After the feature extraction, two independent RPNs, namely image RPN and Doppler RPN, generate a set of rectangular boxes (anchors). In the designed dual Faster R-CNN, the image and Doppler RPNs are trained according to their individual anchors. The loss functions of image and Doppler RPNs are

given by [20]

$$L_{\text{img\_rpn}} = \frac{1}{N_{\text{rpn\_cls}}} \sum_i L_{\text{rpn\_cls}}(p_{Ii}, p_{Ii}^*)$$
$$+ \frac{\lambda}{N_{\text{rpn\_reg}}} \sum_i p_{Ii}^* L_{\text{rpn\_reg}}(t_{Ii}, t_{Ii}^*)$$
$$L_{\text{dop\_rpn}} = \frac{1}{N_{\text{rpn\_cls}}} \sum_j L_{\text{rpn\_cls}}(p_{Dj}, p_{Dj}^*)$$
$$+ \frac{\lambda}{N_{\text{rpn\_reg}}} \sum_j p_{Dj}^* L_{\text{rpn\_reg}}(t_{Dj}, t_{Dj}^*) \quad (1)$$

where $L_{\text{rpn\_cls}}(\cdot)$ is a two-class cross entropy loss function (background versus foreground), p_{Ii} is the predicted probability of anchor i as an object in SAR image, and the ground-truth label p_{Ii}^* is 1 if the anchor is positive, otherwise it is zero. $L_{\text{rpn\_reg}}(\cdot)$ is a regression loss function, which is activated only for positive anchors. t_{Ii} is a vector representing the translation and scaling parameters of the predicted bounding box in SAR image and t_{Ii}^* is that of the ground-truth box (likewise for p_{Dj}, t_{Dj}, p_{Dj}^*, and t_{Dj}^*).

Moreover, the image and Doppler RPNs provide ε precise region proposals to train the subsequent detection network, respectively. The ith region proposal γ_i provided by image RPN and the jth region proposal η_j provided by Doppler RPN can be expressed as

$$\gamma_i = \left[x_{Ii}^1, y_{Ii}^1, x_{Ii}^2, y_{Ii}^2\right], \quad i = 1, \dots, \varepsilon$$
$$\eta_j = \left[x_{Dj}^1, y_{Dj}^1, x_{Dj}^2, y_{Dj}^2\right], \quad j = 1, \dots, \varepsilon \quad (2)$$

where (x_{Ii}^1, y_{Ii}^1) and (x_{Ii}^2, y_{Ii}^2) represent upper-left and lower-right coordinates of the ith region proposal in SAR image (likewise for η_j). Therefore, all region proposals in SAR image and its related RD spectrum are $\Lambda_I = \{\gamma_1, \dots, \gamma_\varepsilon\}$ and $\Lambda_D = \{\eta_1, \dots, \eta_\varepsilon\}$, respectively.

Subsequently, these region proposals are then shifted from one domain to another based on the property that the shadow of a moving target and its Doppler energy are located around the same range. For example, by keeping the range coordinates of region proposals provided by image RPN unchanged, their corresponding region proposals in RD spectrum can be obtained by mapping the azimuth coordinates. In this way, the paired region proposals are obtained in SAR image and RD spectrum with the same range coordinates but the different azimuth coordinates. Similarly, the region proposals provided by Doppler RPN are also shifted to the SAR image.

A rule-based azimuth coordinate shift method is used to generate paired region proposals, which shifts region proposals from one domain to another. This azimuth coordinate shift method is implemented by three steps.

First, the differences of range coordinates between γ_i and all region proposals in Λ_D are calculated. Assume that mth region proposal η_m has the smallest range coordinate difference, which can be calculated by

$$m = \arg\min_j \left[|y_{Ii}^1 - y_{Dj}^1| + |y_{Ii}^2 - y_{Dj}^2|\right]. \quad (3)$$

Second, the region proposal γ_i in SAR image can be shifted to RD spectrum as γ_i' by using the azimuth coordinates of η_m and holding the range coordinates, which can be expressed as

$$\gamma_i' = \left[x_{Dm}^1, y_{Ii}^1, x_{Dm}^2, y_{Ii}^2\right]. \tag{4}$$

Third, all region proposals in Λ_I are shifted to RD spectrum using (3) and (4) (likewise for region proposals in Λ_D). Therefore, the paired region proposals used in the designed dual Faster R-CNN can be expressed as

$$P_I = \{\gamma_1, \ldots, \gamma_\varepsilon, \eta_1', \ldots, \eta_\varepsilon'\}$$
$$P_D = \{\gamma_1', \ldots, \gamma_\varepsilon', \eta_1, \ldots, \eta_\varepsilon\} \tag{5}$$

where γ_1 and γ_1' are a pair of region proposals with the same range coordinates but different azimuth coordinates, P_I contains 2ε region proposals for detection of shadow and masked shadow in the SAR image (likewise for P_D).

Through azimuth coordinate shift, region proposals from two independent RPNs are shared and paired region proposals are obtained for joint detection. As a supervised network, it is necessary to calculate the category label and regression parameter label for each region proposal in P_I and P_D. The overlap ratios between each region proposal and ground-truth boxes of each category in the current image are calculated to decide the category labels [20]. At the same time, the translation and scaling parameters of the positive region proposals are also calculated as the regression parameter labels. These labels are used to train the subsequent detection network.

Two RoI pooling layers are used to extract features with fixed size from their individual feature maps based on P_I and P_D. The fully connected layers are used to classify each pair of region proposals and to predict the regression parameters of bounding boxes. The loss function of the detection network can be written as

$$L_{\text{rcnn}} = \frac{1}{N_{\text{cls}}} \sum_i \left[L_{\text{img\_cls}}(q_{Ii}, q_{Ii}^*) + L_{\text{dop\_cls}}(q_{Di}, q_{Di}^*)\right]$$
$$+ \frac{\lambda}{N_{\text{reg}}} \sum_i \left[q_{Ii}^* L_{\text{img\_reg}}(t_{Ii}, t_{Ii}^*) + q_{Di}^* L_{\text{dop\_reg}}(t_{Di}, t_{Di}^*)\right] \tag{6}$$

where $L_{\text{img\_cls}}(\cdot)$ and $L_{\text{dop\_cls}}(\cdot)$ are three-class (background, shadow, and masked shadow) and two-class (background versus target Doppler) cross entropy loss functions, respectively. $L_{\text{img\_reg}}(\cdot)$ and $L_{\text{dop\_reg}}(\cdot)$ are regression loss functions. Therefore, the total loss of the dual Faster R-CNN can be written as

$$L = L_{\text{img\_rpn}} + L_{\text{dop\_rpn}} + L_{\text{rcnn}}. \tag{7}$$

In the train, some region proposals in Λ_I and Λ_D are gradually concentrated on the real moving target, and thus, the shifted region proposals are also gradually close to the true target in the other domain. Therefore, the paired region proposals are helpful for driving the network to simultaneously detect the moving target around the same range in the SAR image and RD spectrum.

In the test, 2ε pairs of region proposals are output after bounding box regression using the predicted regression parameters. For a pair of region proposals, they can be retained only when

TABLE I
TYPICAL RADAR PARAMETERS FOR SIMULATIONS OF VIDEO SAR DATA

Parameter	Description	Value
Center Frequency	f_c	35 GHz
Bandwidth	B_w	750 MHz
Pulse Repetition Frequency	PRF	3 KHz
Pulse Duration	T_p	20 μs
Sampling Frequency	F_s	30.5 MHz
Grazing Angle	θ	25°
Flight Radius	R	2.5 Km
Flight Velocity	v	45 m/s
Subaperture Length	N	3072
Subaperture Step Length	S	144
Subaperture Numbers	T	200
Doppler Pulse Numbers	K	256
Clutter-to-Noise Ratio	CNR	10~17.5 dB
Signal-to-Clutter Ratio	SCR	-5~0 dB
Scene Size	A_s	120 m × 120 m
Target Size	T_s	3 m ~ 7 m

their classification probabilities are both above the detection threshold. Then, the nonmaximum suppression (NMS) is used to suppress the redundant region proposals in the SAR image, and corresponding region proposals in the RD spectrum are dropped at the same time. Moreover, the NMS is used again in the RD spectrum to further eliminate the overlapping region proposals.

A successful detection can be declared when the shadow of a moving target in the SAR image and its Doppler energy in the RD spectrum are simultaneously detected by a pair of region proposals. This joint detection approach fully uses the target features in both the SAR image and RD spectrum, which enables a good detection performance and significant improvement in false alarm.

IV. EXPERIMENTAL RESULTS

The joint detection of moving target based on dual Faster R-CNN is examined both on the simulated and real video SAR data, and the resulted false alarm and missing alarm are discussed. Meanwhile, the conventional methods, such as the classical Faster R-CNN and the conventional DP-TBD algorithm, are used to detect shadows only in the SAR image for the purpose of comparison.

A. Simulated Video SAR Data

The radar parameters used in the simulations are listed in Table I. The background returns of single channel circular video SAR are generated based on the real SAR reflectivity images. The moving targets are simulated additionally.

The simulation of moving target uses a 2-D model of a real tank SAR image [30]. Its pixel numbers are resized to match different target sizes, and the shape is rotated according to the set motion direction. The moving target echoed signal can be obtained by calculating the summation of returns from all the scatterers on the target model. Targets with different sizes and velocities are used to verify the robustness of the proposed approach. In each set of video SAR returns, the size of the moving target is selected in the range of 3–7 m, and the aspect ratio is adjusted according to the motion direction. Different

TABLE II
TYPICAL SPEED PARAMETERS USED IN SIMULATIONS

Range and azimuth initial velocity v_r and v_a (m/s) Range and azimuth acceleration a_r and a_a (m/s^2)					
Target	Slow-time sample No.	v_r	a_r	v_a	a_a
1	1∼15000	3.50	0.60	1.03	0.30
	15001∼31728	6.50	-0.60	2.53	-0.30
2	1∼12000	-7.00	0.20	-2.04	0
	12001∼24000	-6.20	1.55	-2.04	0.51
	24001∼24900	0	0	0	0
	24901∼31728	0	-1.00	0	-0.40
3	1∼6000	-1.27	0	8.00	0
	6001∼24000	-1.27	-0.70	8.00	-1.60
	24001∼31728	-5.47	-0.70	-1.60	0

motions have been used to simulate the moving targets with various speeds. Some typical speed parameters are illustrated in Table II.

The shadow is simulated as a black area with the same shape and size as the moving target, which is a good approximation under large depression angle. It should be pointed out that even if the sizes of targets are the same, the shapes and sizes of their shadows generated under different speeds are different. After the image formation by the well-known PFA in a subaperture, the length of shadow of a moving target depends on its speed and length along the speed direction [12]. The shadow will expand along the motion direction of the target. For a moving target, the higher the speed, the longer the theoretical length of its shadow. However, as the speed increases, the contrast between the shadow and background decreases due to the shorter occlusion time [10]. A slower target has a more distinct shadow, and the shadow intensity roughly varies with the occlusion time linearly. Therefore, in the focused SAR images, the shadow features are significantly affected by the motion. Different motion states also increase the diversities of shadows. On the other hand, the simulated shadow is different from the real moving target shadow. The main difference is that the real shadow is composed of two parts the occlusion of a moving target to background and the projection of the target with height along radar line of sight. The simulated shadow is based on the former since the real shadow is mainly composed of the former under large grazing angle. In this case, the simulated shadow can reflect most characteristics of the real shadow.

The real SAR reflectivity images for background simulation are shown in Fig. 5, where Fig. 5(a)–(c) is used in the training and testing dataset. The Gaussian complex noise is added into the background returns according to CNR, and then total video SAR returns are obtained by adding the returns of target and its shadow with specified SCR. Each set of video SAR returns contains 200 subapertures, and each subaperture can be used to form a high resolution video SAR image and a low resolution RD spectrum, which are concatenated as one training image. In the training dataset, 600 sets of video SAR returns are simulated and 48 K concatenated images are chose as the training images.

The following four cases are considered in the test to examine the robustness of the proposed approach.

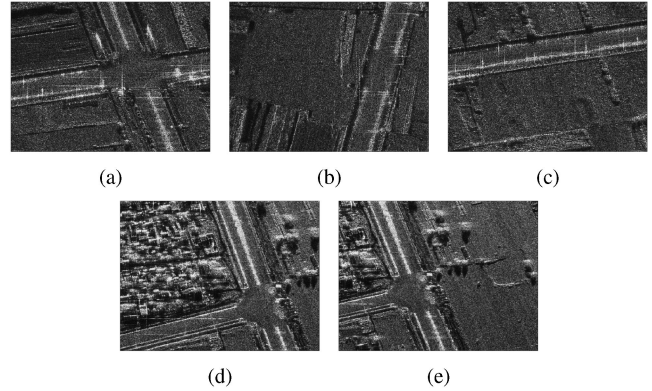1) Case A: using the used scenes in the training dataset.

Fig. 5. Real SAR images used for background returns. (a)–(c) Scenes used in the training and testing set. (d) and (e) Scenes only used in the testing set.

TABLE III
PARAMETERS OF TESTING DATASET

	Images	Targets	Scenes	Resolution
Case A	400	1000	Fig. 5(b) and 5(c)	High
Case B	400	1800	Fig. 5(d) and 5(e)	High
Case C	400	1000	Fig. 5(b) and 5(c)	Low
Case D	400	1000	Fig. 5(d) and 5(e)	Low
All	1600 testing images and 4800 moving targets			

2) Case B: using the unused scenes in the training dataset.
3) Case C: using the used scenes in the training dataset with lower resolutions.
4) Case D: using the unused scenes in the training dataset with lower resolutions.

Typical parameters of the testing dataset are given in Table III. Fig. 5(b) and (c) is used as the backgrounds in Case A, which have been used in the training dataset. There are 400 testing images in Case A including 1000 moving targets. In Case B, Fig. 5(d) and (e) is used as the backgrounds. In particular, these scenes have never been used in the training dataset. Case B contains 400 testing images and 1800 moving targets. The backgrounds of Case C and Case D are the same as those of Case A and Case B, respectively, but using half of the bandwidth, subaperture length, and Doppler pulse numbers to reduce the resolutions. Both Cases C and D contain 400 testing images and 1000 moving targets. Finally, there are total 1600 images and 4800 moving targets in the testing dataset. Some testing images are shown in Fig. 6.

B. Results of Simulated Radar Data

The dual Faster R-CNN is trained using the abovementioned training dataset of 48 K images. During the training stage, the learning rate is set to 0.001, which is an empirical parameter used to train Faster R-CNN in most cases. Meanwhile, the classical Faster R-CNN is trained only using the video SAR images under the same dataset and training parameters for comparison.

Both the dual and classical Faster R-CNNs can locate the positions of shadows in the SAR image using the bounding boxes, and give the classification probabilities at the same time. The larger the classification probability, the higher the
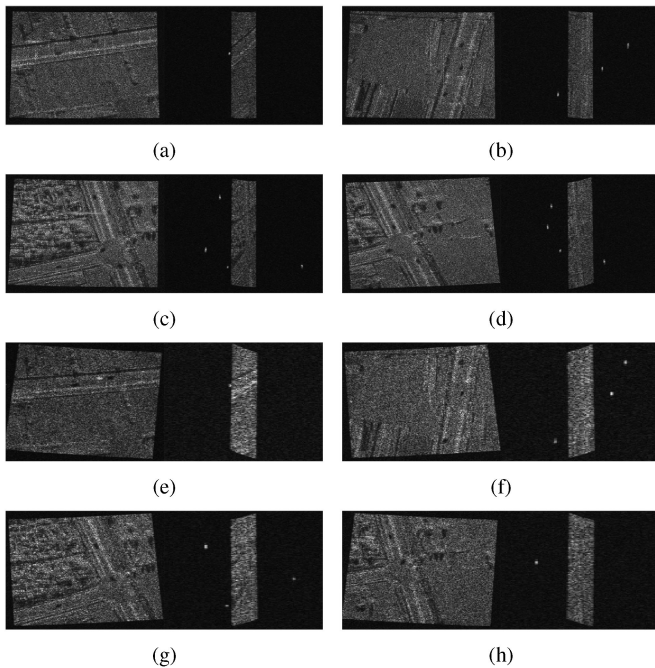
Fig. 6. Some testing images. (a) and (b) Case A. (c) and (d) Case B. (e) and (f) Case C. (g) and (h) Case D.

confidence of the network to recognize the region proposal as the specified object. In the classical Faster R-CNN, the region proposals whose classification probabilities are higher than the detection threshold are output as the final detection results after NMS. However, a pair of region proposals are selected only when their classification probabilities are both higher than the detection threshold in the dual Faster R-CNN, and the final detection results are obtained using NMS in the SAR image and RD spectrum in turns.

Moreover, the conventional DP-TBD algorithm [31] is used to give the comparison of the detection performance. Since the subaperture step length S is quite smaller than the subaperture length N in the simulations, there are slight differences between two adjacent simulated SAR images, which brings difficulties to background extraction and shadow detection. Therefore, all 1600 testing images are divided into 32 groups, and 5 sequential SAR images are selected every 10 frames from a group as a set of image samples for the experiments. In this way, the differences between SAR images to be detected are increased and the moving targets have obvious motions, which is helpful for target tracking and detection. Before the initial detection, the stationary clutter is expected to be suppressed. However, video SAR images are rotated if the spotlight or circular SAR data are focused by the PFA, which needs additional procedures to correct this rotation. Therefore, in the first place, the mean filters are used to suppress the speckle noise and the image registrations are implemented for the first two frames by using the well-known scale-invariant feature transform and the random sample consensus algorithms [14]. In detail, for a set of images to be detected, the fourth and fifth images are registered to the first and second images, respectively. Second, the backgrounds of

the first two frames are extracted and the clutter suppressions are realized by removing the backgrounds. Third, the initial detection procedures are performed by using a two-parameter constant false alarm rate detector and the morphological processing. The centers of the connected components are considered as the detected points. Fourth, the detected points in the first two frames are matched to obtain candidate targets and to estimate the initial states. Finally, the classical DP-TBD algorithm is used to simultaneously detect and track the moving target shadow over five frames by integrating the merit function. Here, we used the pixel value as the merit function, and the pixel value is reversed to change the shadow from dark to bright. The DP-TBD algorithm declares the presence of moving target shadow if the integrated merit function exceeds the set threshold in the last frame.

The detection results using the conventional DP-TBD algorithm, classical Faster R-CNN and the proposed dual Faster R-CNN are shown in Fig. 7. These testing images are all from Case B. In each image, the first and second columns show the detection results obtained from the conventional DP-TBD algorithm and classical Faster R-CNN, respectively. The third column gives the detection results both in the SAR image and RD spectrum using the dual Faster R-CNN. The detection thresholds equal to 0.6 in both the deep learning-based methods, which are the standard thresholds set in the Faster R-CNN [20]. Fig. 7(a), (b), and (f) shows the proposed dual Faster R-CNN has less false alarms than the classical Faster R-CNN. The dual Faster R-CNN uses paired region proposals to jointly detect the moving targets. A target can be considered as a real moving target only if it is detected in both SAR image and RD spectrum. The interference areas whose features are similar to the moving target shadow, such as the shadow of a fixed target, are easy to be misjudged in the SAR image. However, these areas do not have Doppler energy zones as moving target at the corresponding positions in the RD spectrum. Hence, these false alarms can be effectively suppressed. On the other hand, it can be observed that the classical Faster R-CNN generates a large number of false alarms and missing alarms in the testing images come from Case B due to poor generalization ability. The conventional DP-TBD algorithm uses the strategy of integrating the energy of shadows between frames. As shown in Fig. 7(c) and (d), the false alarms are easily generated in the other areas of weak reflectivity. The missing alarm occurs in Fig. 7(e) when the moving target shadow is masked by its Doppler energy.

There are some missing alarms in the detection results of dual Faster R-CNN. The first reason lies in the fact that the stationary clutter is not suppressed in the RD spectrum, which makes it difficult to detect Doppler energy of moving target with the interference of stationary clutter. For a slow moving target with low SCR, the missing alarm easily occurs when its Doppler energy is inside the stationary clutter, as shown in Fig. 7(f). However, in some cases, the dual Faster R-CNN can correctly detect slow moving targets based on its powerful feature extraction abilities. Fig. 7(c) and (d) shows the correct detections of slow moving targets in the stationary clutter. The second is that when two detection results are located at the adjacent range, the false alarm and missing alarm likely occur. In Fig. 7(e), there are a
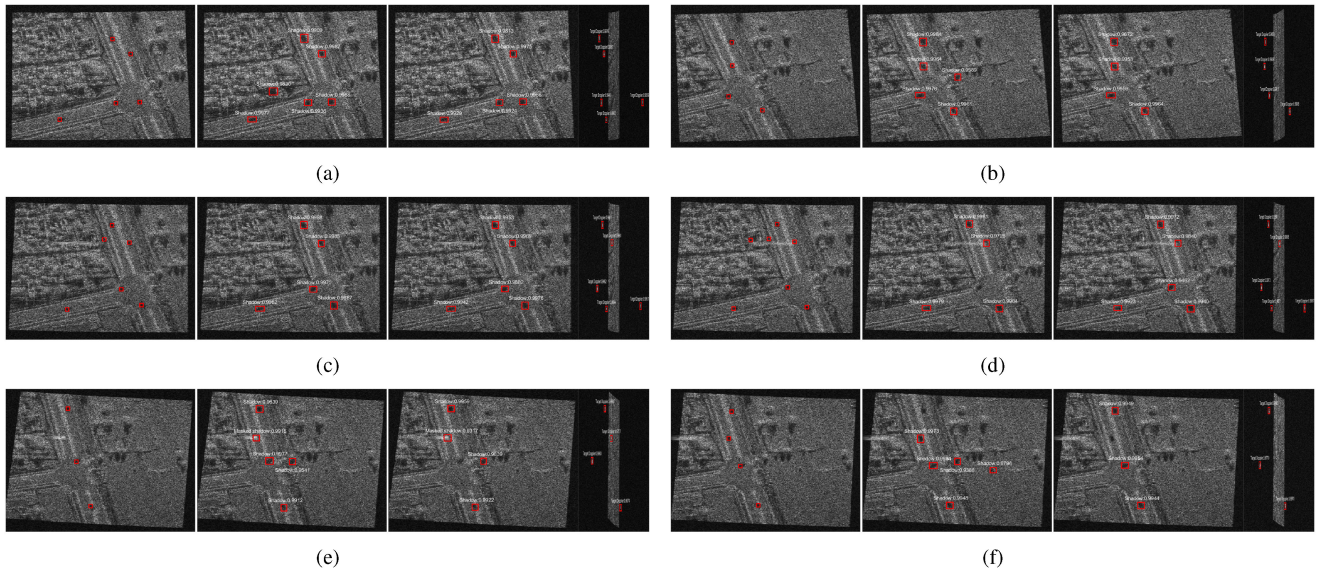
Fig. 7. Comparisons of the detection results of the simulated video SAR data. (a)–(f) Detection results of different testing images from Case B. In each image, the first and second columns show the detection results obtained from the conventional DP-TBD algorithm and classical Faster R-CNN, respectively. The third column gives the detection results both in the SAR image and RD spectrum using the dual Faster R-CNN. In the deep learning-based methods, a detection threshold of 0.6 is used to display these results.

false alarm and a missing alarm in the detection results of the dual Faster R-CNN. The corresponding region proposal of the false alarm also detects the Doppler energy of target in the RD spectrum, and its classification probability happens to be higher than that of the corresponding region proposal of moving target shadow. In this case, after NMS in the RD spectrum, the false alarm is retained while the shadow is removed.

However, the paired region proposals are useful for network to search the moving target around the same range, which has some improvements in the missing alarm. As shown in Fig. 7(d) and (f), there are two missing alarms in the detection results of the classical Faster R-CNN. In our approach, a region proposal correctly covers the Doppler energy of target in the RD spectrum, and its corresponding region proposal in the SAR image forces the network to search potential targets around the same range. Therefore, the dual Faster R-CNN can successfully detect these moving targets based on the paired region proposals. The joint detection can also be implemented by two independent Faster R-CNNs, which detect shadow and Doppler energy in the SAR image and RD spectrum, respectively. The preliminary detection results can be associated for final decisions. However, this method does not use the paired region proposals in the training stage, and cannot drive the network to simultaneously detect the moving targets around the same range. It is obvious that the method of associating independent detection results can only suppress false alarms but has no improvement on missing alarms, which are worse than the classical and dual Faster R-CNNs.

All the detection results of different methods using the simulated testing dataset are illustrated in Table IV, which gives the comparisons of the detection performance in terms of false alarm, missing alarm, average number of false alarms per frame (NFA) and the probability of detection (PD). The number of testing images is 1600, which contains 4800 moving targets.

TABLE IV
COMPARISONS OF DETECTION PERFORMANCES OF DIFFERENT METHODS USING SIMULATED DATA WITH DETECTION THRESHOLD OF 0.6

Approach	False	Missing	NFA	PD (%)
DP-TBD algorithm	89	239	0.0556	95.02
Classical Faster R-CNN	298	219	0.1862	95.44
Dual Faster R-CNN	**26**	**232**	**0.0163**	**95.17**

The bold entities are used to intuitively illustrate the detection performance of our proposed method.

The detection threshold of 0.6 is used for both the classical and dual Faster R-CNN. The proposed approach shows much better detection performance compared to the other methods in terms of false alarms. The number of false alarms of the conventional DP-TBD algorithm and the classical Faster R-CNN is about 3.4 and 11.5 times of our approach, respectively, which indicates our joint detection approach has better control of false alarm in video SAR moving target detection. The performance of classical Faster R-CNN is deteriorated due to the poor generalization ability. Although the paired region proposals have some contributions in searching the moving target, our approach has no noticeable advantage in missing alarms due to the stricter detection conditions. The number of missing alarms in our approach is 232, which is more than the classical Faster R-CNN, however, the detection probability can reach 95.17% with less false alarms. Therefore, the dual Faster R-CNN is superior to the other two conventional methods. Furthermore, the influence of detection threshold is considered, and the comparisons of detection performances of deep learning-based methods under different detection thresholds are illustrated in Table V. It can be seen that with the increase of detection threshold, the number of false alarms decreases while the number of missing alarms increases.

TABLE V
COMPARISONS OF DETECTION PERFORMANCES USING SIMULATED DATA UNDER DIFFERENT DETECTION THRESHOLDS

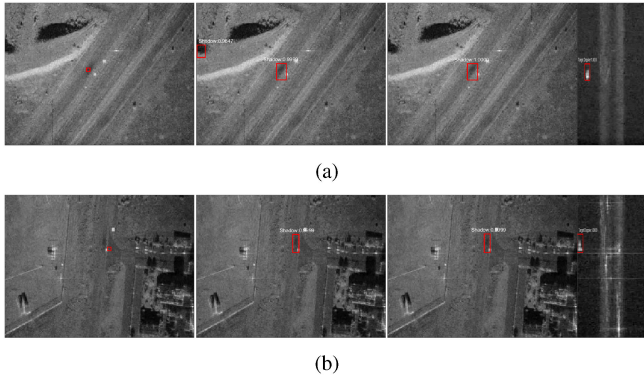| Detection Threshold	Dual Faster R-CNN		Classical Faster R-CNN	
	False	Missing	False	Missing
0.6	26	232	298	219
0.7	19	261	271	240
0.8	11	290	223	283

(a)

(b)

Fig. 8. Comparisons of detection results of the real video SAR data. The first and second columns show detection results obtained from the conventional DP-TBD algorithm and classical Faster R-CNN, respectively. The third column gives the detection results both in the SAR image and RD spectrum using the dual Faster R-CNN. In the deep learning-based methods, a detection threshold of 0.6 is used to display these results.

A comparison of the computational loads is briefly discussed, where the experiments are performed on the platform with a 3.4 GHz CPU. The parameters of our method are at least twice than those of the classical Faster R-CNN due to the dual network structure, which results in higher computational complexity. The mean testing time of our method is 2.9666 s for each frame while the classical Faster R-CNN costs 1.2838 s. The computational complexity of DP-TBD algorithm mainly comes from the image registration and background extraction, which costs 14.4685 s for the first two frames with the sizes of 656×875, and the mean time of subsequent detection for each frame is 2.9358 s.

C. Results of Real Video SAR Data

The real SAR video released by the Sandia National Laboratory [28] has been used to verify the proposed approach. The real video SAR images are extracted every 10 frames from the original data, and 314 frames can be obtained where 224 frames are used as the basic images of training dataset and 90 frames are used as the testing dataset. The original video SAR images are cropped into two parts SAR image and RD spectrum. The frequently used translation has been used to expand the training data, and 32 256 images are obtained as the training dataset. The proposed dual Faster R-CNN is trained using the images concatenated by the SAR image and RD spectrum, and the classical Faster R-CNN and DP-TBD algorithm are also experimented on the SAR image.

There are 90 moving targets in the testing dataset. Fig. 8 shows the detection results of the real video SAR data. The detection thresholds are both 0.6 in the dual and classical Faster R-CNNs.

TABLE VI
COMPARISONS OF DETECTION PERFORMANCES OF DIFFERENT METHODS USING REAL VIDEO SAR DATA WITH DETECTION THRESHOLD OF 0.6

Approach	False	Missing	NFA	PD (%)
DP-TBD algorithm	12	13	0.1333	85.56
Classical Faster R-CNN	4	0	0.0444	100.00
Dual Faster R-CNN	**0**	**1**	**0**	**98.89**

The bold entities are used to intuitively illustrate the detection performance of our proposed method.

TABLE VII
COMPARISONS OF DETECTION PERFORMANCES USING REAL VIDEO SAR DATA UNDER DIFFERENT DETECTION THRESHOLDS

Detection Threshold	Dual Faster R-CNN		Classical Faster R-CNN	
	False	Missing	False	Missing
0.6	0	1	4	0
0.7	0	1	3	0
0.8	0	1	3	0

The conventional DP-TBD algorithm detects the moving target shadow in the successive five frames. Since the changes of beam direction bring difficulties to the DP-TBD algorithm, a common SW processing is used, and the step of the window equals to 1. After the detection, a subsequent filter is used to associate tracks detected in each window [32]. In this article, a simple strategy is adopted for the subsequent filter. In each frame, among the repeated states belonging to the same moving target, only the state with the largest reversed pixel value is retained. Therefore, the repetitive detections are eliminated.

In video SAR image, the region proposal that covers the weak reflectivity area may have similar features as that covers the shadow of moving target, for instance, the intensity, size, and shape. In this case, the classical Faster R-CNN may cause misjudgment, which generates a false alarm in Fig. 8(a). On the other hand, the DP-TBD algorithm fails to detect the shadow in Fig. 8(b), and simultaneously generates a false alarm and a missing alarm. In particular, our approach can still maintain a great detection performance by simultaneously using the features of moving target shadow and Doppler energy. The detection performances of three methods using real video SAR data are illustrated in Table VI. Note that there is only one moving target in each testing image, its shadow is clear in the SAR image and has never been masked, leading to a good detection performance for classical and dual Faster R-CNNs. However, the changes of beam direction deteriorate the detection performance of the DP-TBD algorithm. Table VII shows the comparisons of the detection performance using real video SAR data under different detection thresholds.

Moreover, Fig. 9 shows the comparisons of shadow detection performances of deep learning-based methods varying with the number of training images. In the testing, 90 real images are used and the detection threshold equals to 0.6. In the training of classical and dual Faster R-CNNs, one image is fed into the network for each iteration and the network is saved every 5000 iterations. Therefore, the training images are reused after 32 256 iterations. Particularly, the detection results of deep learning-based methods in Fig. 8, Tables VI and VII are obtained by using 40 000 training images. It can be noticed that false alarms
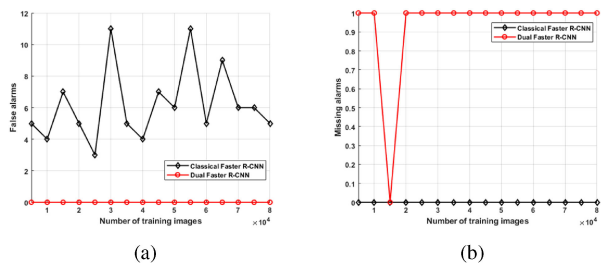
Fig. 9. Comparisons of shadow detection performances of deep learning-based methods varying with the number of training images. In total, 90 real images are tested and the detection threshold equals to 0.6. (a) False alarms. (b) Missing alarms.

of the proposed approach are less than that of the classical Faster R-CNN under different numbers of training images with acceptable missing alarms. Therefore, the proposed dual Faster R-CNN is an effective approach for shadow detection.

V. CONCLUSION

This article presents a new joint moving target detection approach for video SAR using the dual Faster R-CNN, which algorithmically combines the shadow detection in SAR image and the Doppler energy detection in the RD spectrum. The detection performance is significantly improved by using diverse features from different domains.

A rule-based azimuth coordinate shift method is used in the dual Faster R-CNN to share the region proposals of two independent RPNs, and thus, the paired region proposals are obtained. Therefore, a detection can be declared if the shadow of a moving target and its Doppler energy are simultaneously detected in the SAR image and the RD spectrum. Compared to the classical DP-TBD algorithm and Faster R-CNN for shadow-based detection, the proposed approach can effectively suppress false alarm at an acceptable level of missing alarm, which can be further balanced if necessary.

REFERENCES

[1] J. Miller, E. Bishop, and A. Doerry, "An application of backprojection for video SAR image formation exploiting a subaperture circular shift register," *Proc. SPIE*, vol. 8746, May 2013, Art. no. 874609.

[2] A. Damini, B. Balaji, C. Parry, and V. Mantle, "A VideoSAR mode for the X-band wideband experimental airborne radar," *Proc. SPIE*, vol. 7699, Apr. 2010, Art. no. 76990E.

[3] B. Liu, X. Zhang, K. Tang, M. Liu, and L. Liu, "Spaceborne video-SAR moving target surveillance system," in *Proc. IEEE Int. Geosci. Remote Sens. Symp.*, 2016, pp. 2348–2351.

[4] A. Damini, V. Mantle, and G. Davidson, "A new approach to coherent change detection in VideoSAR imagery using stack averaged coherence," in *Proc. IEEE Radar Conf.*, Ottawa, ON, USA, 2013, pp. 1–5.

[5] S. Kim, R. Fan, and F. Dominski, "ViSAR: A 235 GHz radar for airborne applications," in *Proc. IEEE Radar Conf.*, Oklahoma City, OK, USA, 2018, pp. 1549–1554.

[6] X. Song and W. Yu, "Processing video-SAR data with the fast back-projection method," *IEEE Trans. Aerosp. Electron. Syst.*, vol. 52, no. 6, pp. 2838–2848, Dec. 2016.

[7] R. Hu, R. Min, and Y. Pi, "Interpolation-free algorithm for persistent multi-frame imaging of video-SAR," *IET Radar, Sonar Navigat.*, vol. 11, no. 6, pp. 978–986, Jun. 2017.

[8] E. Bishop, R. Linnehan, and A. Doerry, "Video-SAR using higherorder taylor terms for differential range," in *Proc. IEEE Radar Conf.*, May 2016, pp. 1–4.

[9] A. M. Raynal, D. L. Bickel, and A. W. Doerry, "Stationary and moving target shadow characteristics in synthetic aperture radar," *Proc. SPIE*, vol. 9077, May 2014, Art. no. 90771B.

[10] J. Ding, L. Wen, C. Zhong, and O. Loffeld, "Video SAR moving target indication using deep neural network," *IEEE Trans. Geosci. Remote Sens.*, vol. 58, no. 10, pp. 7194–7204, Oct. 2020.

[11] H. Xu, Z. Yang, M. Tian, Y. Sun, and G. Liao, "An extended moving target detection approach for high-resolution multichannel SAR-GMTI systems based on enhanced shadow-aided decision," *IEEE Trans. Geosci. Remote Sens.*, vol. 56, no. 2, pp. 715–729, Feb. 2018.

[12] J. Ding, "Focusing algorithms and moving target detection based on video SAR," (in Chinese), *J. Radars*, vol. 9, no. 2, pp. 321–334, 2020,

[13] Z. Liu, D. An, and X. Huang, "Moving target shadow detection and global background reconstruction for VideoSAR based on single-frame imagery," *IEEE Access*, vol. 7, pp. 42418–42425, 2019.

[14] Y. Zhang, X. Mao, H. Yan, D. Zhu, and X. Hu, "A novel approach to moving targets shadow detection in VideoSAR imagery sequence," in *Proc. IEEE Int. Geosci. Remote Sens. Symp.*, Jul. 2017, pp. 606–609.

[15] H. Wang, Z. Chen, and S. Zheng, "Preliminary research of low-RCS moving target detection based on ka-band video SAR," *IEEE Geosci. Remote Sens. Lett.*, vol. 14, no. 6, pp. 811–815, Jun. 2017.

[16] X. Tian, J. Liu, M. Mallick, and K. Huang, "Simultaneous detection and tracking of moving-target shadows in ViSAR imagery," *IEEE Trans. Geosci. Remote Sens.*, vol. 59, no. 2, pp. 1182–1199, Feb. 2021.

[17] Z. Xu, J. Sun, and F. Wu, "A novel IMM filter for VideoSAR ground moving target tracking," in *Proc. 6th Asia-Pac. Conf. Synthetic Aperture Radar*, Xiamen, China, 2019, pp. 1–5.

[18] R. Girshick, J. Donahue, T. Darrell, and J. Malik, "Rich feature hierarchies for accurate object detection and semantic segmentation," in *Proc. IEEE Conf. Comput. Vis. Pattern Recognit.*, 2014, pp. 580–587.

[19] R. Girshick, "Fast R-CNN," in *Proc. IEEE Int. Conf. Comput. Vis.*, 2015, pp. 1440–1448.

[20] S. Ren, K. He, R. Girshick, and J. Sun, "Faster R-CNN: Towards real-time object detection with region proposal networks," *IEEE Trans. Pattern Anal. Mach. Intell.*, vol. 39, no. 6, pp. 1137–1149, Jun. 2017.

[21] K. Kang et al., "T-CNN: Tubelets with convolutional neural networks for object detection from videos," *IEEE Trans. Circuits Syst. Video Technol.*, vol. 28, no. 10, pp. 2896–2907, Oct. 2018.

[22] W. Han et al., "Seq-NMS for video object detection," 2016, *arXiv:1602.08465*.

[23] Y. Zhang, S. Yang, H. Li, and Z. Xu, "Shadow tracking of moving target based on CNN for video SAR system," in *Proc. IEEE Int. Geosci. Remote Sens. Symp.*, 2018, pp. 4399–4402.

[24] Z. Cui, X. Wang, N. Liu, Z. Cao, and J. Yang, "Ship detection in large-scale SAR images via spatial shuffle-group enhance attention," *IEEE Trans. Geosci. Remote Sens.*, vol. 59, no. 1, pp. 379–391, Jan. 2021.

[25] Y. Chung, P. Chou, M. Yang, and H. Chen, "Multiple-target tracking with competitive hopfield neural network based data association," *IEEE Trans. Aerosp. Electron. Syst.*, vol. 43, no. 3, pp. 1180–1188, Jul. 2007.

[26] Z. Liu, D. K. C. Ho, X. Xu, and J. Yang, "Moving target indication using deep convolutional neural network," *IEEE Access*, vol. 6, pp. 65651–65660, 2018.

[27] G. D. Martin, A. W. Doerry, and M. W. Holzrichter, "A novel polar format algorithm for SAR images utilizing post azimuth transform interpolation," Sandia National Laboratories, Albuquerque, NM, USA, Sandia Rep. SAND2005-5510, Sep. 2005.

[28] Sandia National Laboratories, "Velocity independent continuous tracking radar mode." Accessed: Dec. 2019. [Online]. Available: http://www.sandia.gov/radar/_assets/videos/victr.mp4

[29] K. Simonyan and A. Zisserman, "Very deep convolutional networks for large-scale image recognition," 2015, *arXiv:1409.1556*.

[30] M. Soumekh, *Synthetic Aperture Radar Signal Processing*. New York, NY, USA: Wiley, 1999.

[31] W. Yi, M. R. Morelande, L. Kong, and J. Yang, "An efficient multi-frame track-before-detect algorithm for multi-target tracking," *IEEE J. Sel. Topics Signal Process.*, vol. 7, no. 3, pp. 421–434, Jun. 2013.

[32] J. Wang, W. Yi, T. Kirubarajan, and L. Kong, "An efficient recursive multiframe track-before-detect algorithm," *IEEE Trans. Aerosp. Electron. Syst.*, vol. 54, no. 1, pp. 190–204, Feb. 2018.

Liwu Wen received the B.Eng. degree in electronic engineering in 2018 from Xidian University, Xi'an, China, where he is currently working toward the Ph.D. degree in the area of radar imaging.

Jinshan Ding (Member, IEEE) is currently a Professor with the School of Electronic Engineering, Xidian University, Xi'an, China. He founded the millimeter-wave and THz Research Group with the Xidian University in 2014. His research interests include millimeter-wave and THz radar, video SAR, and machine learning in radar.

Otmar Loffeld (Senior Member, IEEE) received the Diploma degree in electrical engineering from the Technical University of Aachen, Aachen, Germany, in 1982 and the Eng.Dr. and the Habilitation degrees in the field of digital signal processing and estimation theory from the University of Siegen, Siegen, Germany, in 1986 and 1989, respectively.

Since 1991, he has been a Professor of Digital Signal Processing and Estimation Theory with the University of Siegen, Siegen, Germany. In 1999, he was a Principal Investigator (PI) on baseline estimation for X-band part of the Shuttle Radar Topography Mission (SRTM). He lectures on general communication theory, digital signal processing, stochastic models, estimation theory, and synthetic aperture radar. Since 2005, he has been the Chairman of the Center for Sensorsystems (ZESS), University Siegen. He was a PI for interferometric techniques in the German TerraSAR-X mission, and a PI for a bistatic spaceborne airborne experiment. He was a PI in the TerraSAR-X add-on for Digital Elevation Measurement mission and in bistatic Hitchhiker experiments with stationary receiver and TerraSAR-X illuminator. He founded the International Postgraduate Program Multi Sensorics, University of Siegen, in 2002, and in 2008, he established the North Rhine-Westphalia Research School on Multi Modal Sensor Systems for Environmental Exploration and Safety.

Prof. Loffeld is a member of the Information Technology Society (ITG/VDE) and a senior member of the IEEE Geoscience and Remote Sensing Society.